ACS OMEGA

Open Access

http://pubs.acs.org/journal/acsodf

Article

Influence of Mineral Composition on Rock Mechanics Properties and Brittleness Evaluation of Surrounding Rocks in Soft Coal Seams

Dun Wu, Bo Li, Jian Wu,* Guangqing Hu,* Xia Gao, and Jianwei Lu

Cite This: *ACS Omega* 2024, 9, 1375−1388

Read Online

ACCESS | Metrics & More | Article Recommendations

ABSTRACT: The structural fracture of the coal seam with its low permeability is the dominant reason for the "difficult gas out" of the broken soft coal seam. The brittleness of the roof and floor rock stratum of the broken soft coal seam has a significant effect on the fracture extension pressure of the surrounding rock after casing perforation and hydraulic fracturing of the horizontal well for coalbed methane (CBM). In this paper, 15 rock samples were scientifically collected from the roof and floor of the main mining coal seam of the Early Permian coal-bearing series in the Xinxie-1 well of the Huainan Coalfield in Anhui Province, China. On the basis of mineral composition analysis of these samples, the influence of mineral composition on the mechanics properties of the rock at the roof and floor of the coal seam was investigated. The correlation analysis and gray correlation analysis were adopted to construct an evaluation method for the brittleness of the rock at the roof and floor of the coal seam based on the mineral content. The results indicated that the most significant compositions of the minerals in the rock at the roof and floor of the broken soft coal seam were quartz and clay minerals. The most significant types of rock cementation are quartz agglomeration and rhodochrosite cementation. Pore destruction as a result of cementation was much greater than that of compaction. In comparison to clay minerals, the variation in the content of brittle minerals such as quartz, plagioclase, and siderite in the rock showed more sensitivity to the mechanics properties of the rock. The more sensitive minerals for compressive strength (CS), shear strength (SS), modulus of elasticity (E), softening coefficient (K), and Poisson's ratio (μ) are quartz, those for tensile strength (TS) are plagioclase and siderite, and those for Poisson's ratio are clay minerals. Based on the established mineral content weighting analysis method, it was calculated that the brittleness index (BI) of the rocks at the roof of the 13-1, 11-2, 9-2, and 4-2 coal seams was larger, which was advantageous for the formation of longer fracturing crack networks. This is theoretical guidance for the optimization of horizontal well fracturing design in the deep coal beds of the Huainan Coalfield.

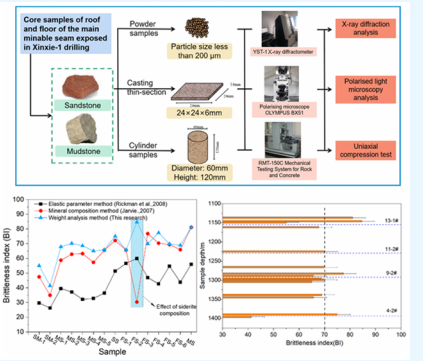

1. INTRODUCTION

At present, the exploration and development of clean energy such as unconventional natural gas (shale gas, coalbed gas, and tight sandstone gas) has become a hot topic in energy science in the world today.[1−3] Lianghuai coalfield in Anhui Province is the most important coal production base in eastern China. The potential of coalbed methane resources is huge, and the geological resources of coalbed methane can reach 90 million cubic meters. However, the broken soft coal seams are extremely developed in the Lianghuai coalfield. The so-called "broken soft coal seam" refers to the coal seam where the original natural fracture network system was destroyed or even disappeared under the action of structural compression and shear stress and the coal structure was characterized by broken block, fragmented, powder, scale, and so on. Compared with a hard coal seam, the development of coalbed gas in a broken soft coal seam was more difficult. A broken soft coal seam was characterized by broken, soft, and low permeability; it was "difficult to release gas" and rapid productivity attenuation in coalbed gas development. Conventional fracturing along a structural coal reservoir is not effective,[4] but the fracturing along the roof and floor of the coal seam have achieved initial results. For example, the LG drilling group of Luling coal mine, Huaibei coalfield, Anhui Province (Figure 1) had a daily gas production of 10,000 m^3 and a stable production of 3000 m^3/d in 100 days.[5,6] Therefore, for the traditional coalbed gas development, the parameters such as coal quality, gas content, and reservoir physical properties (porosity, permeability) of coal reservoirs became the key parameters of coalbed gas reservoir evaluation. For the development of coalbed gas in a broken soft coal seam, special attention was paid to the evaluation and research of key parameters of reservoir fracturing such as mineralogy, petrology and engineering mechanics of the roof and floor of the coal seam.[7−9]

Received: October 5, 2023
Revised: October 30, 2023
Accepted: December 7, 2023
Published: December 29, 2023

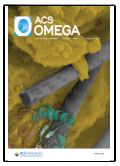

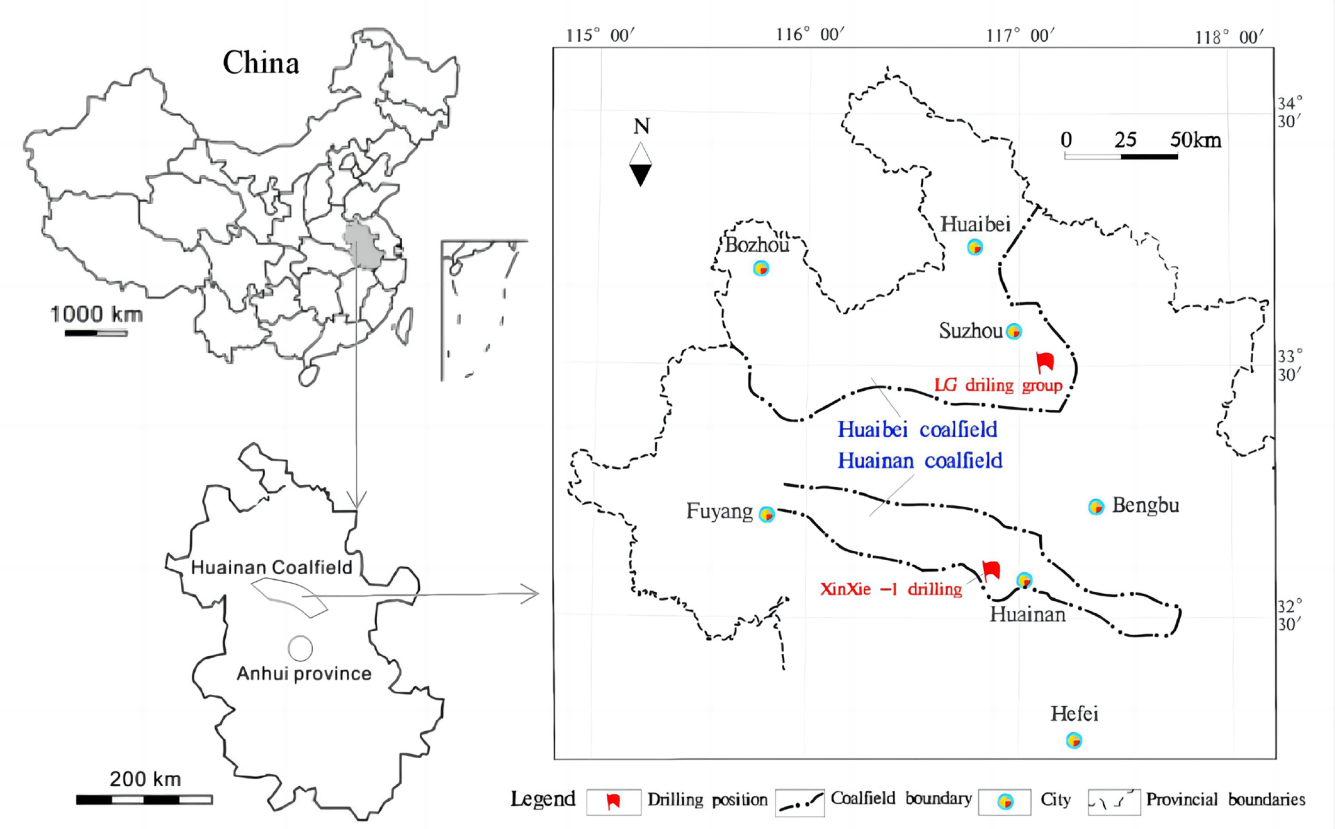

Figure 1. Physical geography map of the study area. The location of the Xinxie-1 well is presented in this figure.

The composition of the material in the coal seam is very complex, and the minerals in it consist mainly of quartz, pyrite and other sulfides, dolomite, siderite and other carbonates, and a range of other clay minerals.[10] There are significant variations in the mineral composition and content of different coal seams due to differences in a variety of factors such as geographic location and depositional environments. For example, synsedimentary volcanic ash causes geochemical and mineralogical anomalies in coal seams.[11] Minerals in the M9 coal from the Yanshan Coalfield in the Yunnan Province, southwestern China, are mainly high-temperature quartz, diabase, dolomite, limonite, Illite, and pyrite.[12] Mineral composition affects the mechanical properties of rocks at the top and bottom of coal seams. Jarvie et al.[13] in their study of shale, noted that quartz can effectively respond to some of the properties of shale. However, in addition to quartz, other carbonate minerals should not be ignored. The mineral composition of shale from the Longmaxi Formation in the Weiyuan area of the Sichuan Basin has a high calcite and dolomite content, which also plays an important role in the overall brittleness of the shale.[14]

Not only are the minerals in a rock complex and variable,[15,16] but also the different cementation states may have a significant effect on its various properties.[17,18] In view of different diagenetic facies that had different petrology, diagenesis, and physical properties,[19,20] these characteristics directly determine the size of rock mechanics parameters (including compressive strength, Poisson's ratio, and elastic modulus) and the reasonable evaluation of rock brittleness.[21] It is of great significance to the effective prediction of formation fracture pressure and the evaluation of wellbore stability during coalbed methane development.

The brittleness index of the fractured reservoir in the coal seam top was an important evaluation index that determined the fracturing effect and gassed production effect of coalbed gas.[8,9,22] According to Liu et al.,[23] there were many factors affecting the brittleness of rock, and it was generally believed that the brittleness of rock was related to mineral composition and rock mechanics properties. However, there was no consistent definition of brittleness index in the literature, resulting in different quantitative methods.[8,24] According to literature research, the current evaluation methods of brittleness index include dozens of methods based on rock strength or firmness coefficient, rock mechanics properties, mineral composition and content, stress−strain relationship, and so on.[8,13,24−26] Among them, the most representative brittleness evaluation methods are mainly the rock stress−strain relationship method, the brittle mineral method, and the comprehensive evaluation method.[27] The stress−strain relationship of rock includes not only the energy conversion from stress loading to rock fracturing but also other important mechanics properties, such as strength, strain, hardness, modulus (elastic modulus, postpeak modulus, etc.), Poisson's ratio, internal friction angle, cohesion, and so on. Based on these parameters, various methods for calculating rock brittleness are derived. In the concrete calculation process, the adaptability of the calculation formula should be considered reasonably.[28−32] For example, the elastic parameter method is commonly used to continuously calculate the brittleness of rocks, which held that the higher the elastic modulus, the lower the Poisson's ratio. However, this method has its shortcomings. First, the maximum and minimum values of elastic modulus were difficult to determine.[25] Second, the weight of the elastic modulus and Poisson's ratio in brittleness

https://doi.org/10.1021/acsomega.3c07731
ACS Omega 2024, 9, 1375−1388

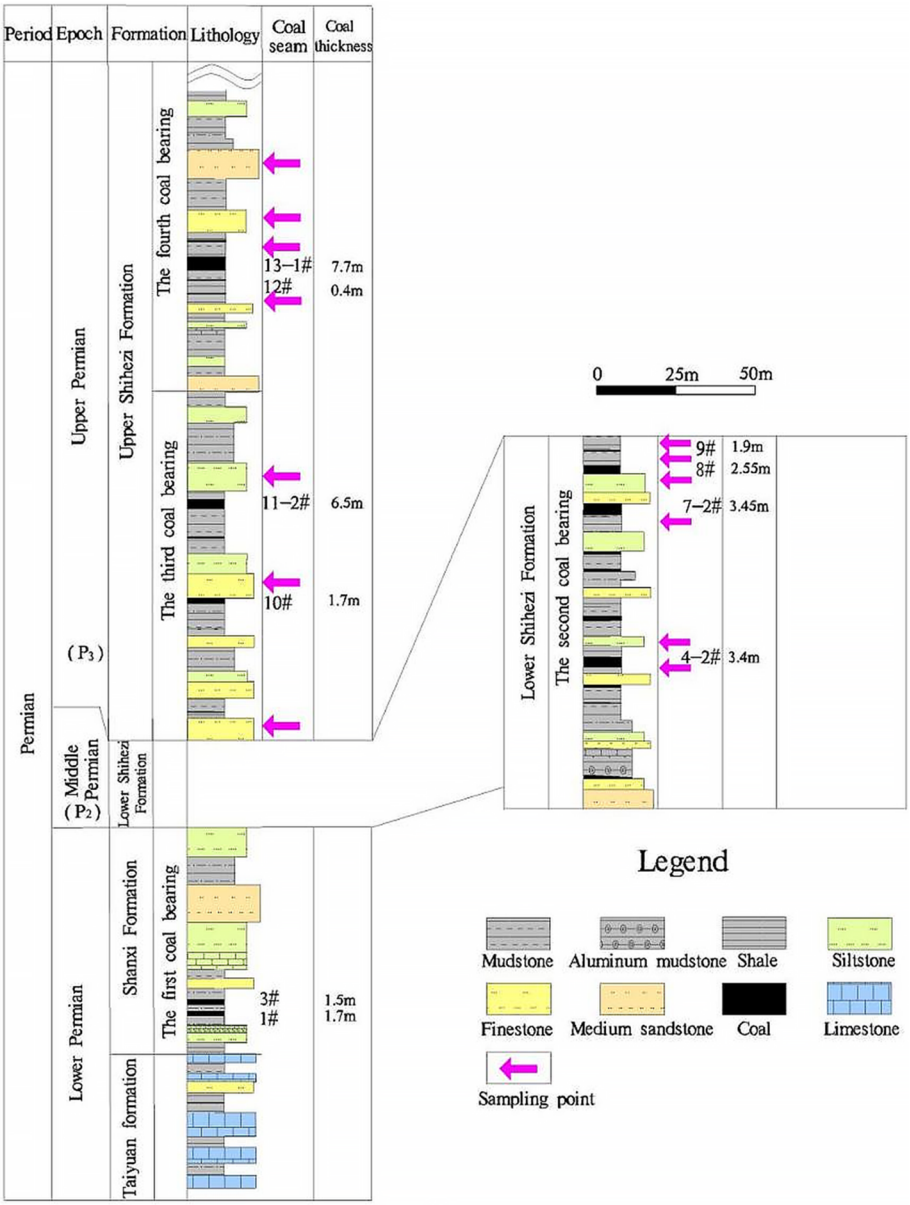

Figure 2. Schematic diagram of the roof and floor of the coal seam sampling.

evaluation was uncertain, which made brittleness evaluation uncertain. Another method was rock mineralogy,[33,34] but this method did not fully consider the influence of other brittle minerals on rock mechanics parameters. The brittleness of rock was related not only to the basic mineral composition but also to its mechanics properties. Brittle minerals make an important contribution to rock fracture formation and evolution; therefore, it is also necessary to determine the brittle minerals in coal seams. Rocks with a high content of brittle minerals usually have mechanical properties with high Young's modulus and low Poisson's ratio. Different regions have different types of brittle minerals, which are related to the sedimentary background, lithology, and facies type.[35] Therefore, when calculating the brittleness of shale in different regions, the calculation method should be chosen according to the actual geological conditions. In addition, the definition of brittle minerals was vague, and it was still controversial whether feldspar minerals and carbonate minerals are identified as brittle minerals.[36,37]

It is not sufficient to estimate the brittleness of shale using rock mechanics or brittle minerals; even if the rocks have the same mineral composition, their porosity, density, and other characteristics can vary significantly after undergoing different diagenetic processes. In addition, brittleness is affected by the diameter of the mineral grains and the degree of cementation in the rock. However, the traditional brittleness evaluation method based on elastic parameters and mineral composition analysis was limited by the anisotropic petrophysical behavior of reservoirs and lacks universal applicability and feasibility.[38] So, it was necessary to comprehensively judge the response law of rocks and minerals in combination with the mechanical properties of rocks. Therefore, this study intended to take Xinxie-1 well (CBM parameter drilling) (Figure 1) in Huainan Coalfield as an example and revealed the geological occurrence law of rock mineral compositions in coal measures strata through experimental research on the roof and floor system of broken soft coal seams in the study area. The response of mineral composition to mechanical properties of coal seam

https://doi.org/10.1021/acsomega.3c07731
ACS Omega 2024, 9, 1375−1388

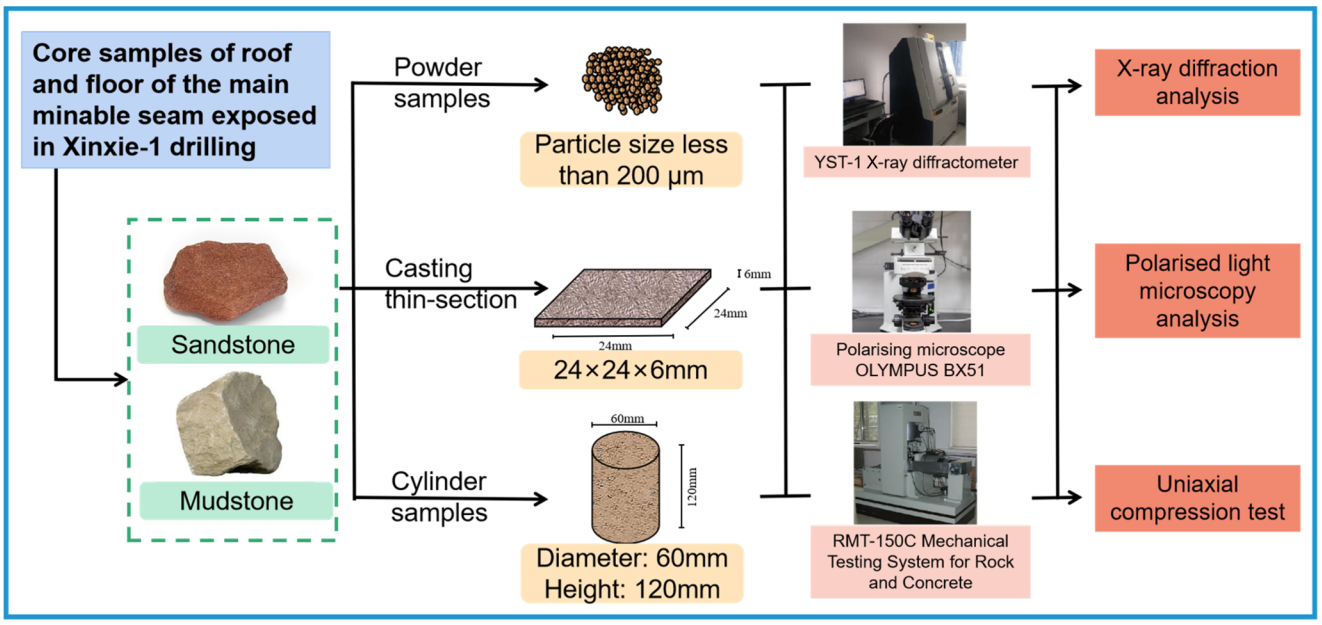

Figure 3. Schematic diagram of the experimental program.

roof and floor rocks was expounded, and the brittleness evaluation method of coal seam roof and floor based on rock mineral composition was established. It provided guidance for the development practice of coalbed methane in the broken soft coal seam development area.

2. MATERIALS AND METHODS

2.1. The Geological Background of the Study Area. Huainan Coalfield was located in the southeast margin of North China's craton on the large tectonic site, and the whole interior showed a complex syncline structural belt complicated by a series of secondary folds. The main coal-bearing strata in Huainan Coalfield include Permian Shanxi Formation, Upper Shihezi Formation, and lower Shihezi Formation. Xinxie-1 well was located in the monoclinal structure of the south wing of the Huainan Hedging Fault Basin, and the drilled strata were Quaternary, Neogene, Paleogene, Triassic, Permian, and Carboniferous. The final hole depth of the Xinxie-1 well was 1541.61 m, and the final hole horizon was Carboniferous-Permian Taiyuan Formation seventh limestone. A total of 30 layers of coal had been discovered by drilling, including 16 minable coal seams, among which 4 stable minable coal seams were 13-1#, 11-2#, 8#, and 7#. The main lithology of the roof and floor of the drilled coal seam were mudstone, sandy mudstone, argillaceous siltstone, siltstone, fine sandstone, and medium sandstone.

2.2. Sample Collection. This study focused on sampling and field description of the core samples of the roof and floor of the main minable seam exposed in the Xinxie-1 well (Figure 2). There are 15 samples, and the length of the samples should be greater than 300 mm (core diameter 60 mm). There were 15 core samples collected this time, and the length of the samples was more than 300 mm (core diameter 60 mm). The structure of the core samples was complete and representative. After the dirt on the surface of the samples was cleaned on site, the samples were sealed and sent to the laboratory for later use. The subsequent experimental procedure is shown in Figure 3.

2.3. X-ray Diffraction Analysis. The mineral composition identification and quantitative analysis of the samples were carried out via a YST-1 X-ray diffractometer. The weight of the sample to be measured is approximately 15 mg. The dried rock samples are ground until the total particle size is less than 40 μm, and the X-ray diffraction data of the samples are compared with the standard X-ray diffraction data of minerals, so as to accurately identify the types of minerals in the samples. The total amounts of clay minerals and nonclay minerals are determined by the corresponding methods, respectively. The experimental test process was carried out with reference to the oil and gas industry standard of the People's Republic of China (SY-T6210-1999).

2.4. Casting Thin-Section. A ZT-3 rock casting instrument was used to prepare the rock casting sheet. First, the project team selected representative parts of rock samples to be measured and cut them into squares of 24 × 24 × 6 mm^3, put the samples in a drying oven for 4 h, controlled the temperature between 105 and 110 °C, dried the moisture, and put them into a dryer for later use after natural cooling. Second, the prepared dyeing resin was injected into the sample tube, and the sample was submerged for more than 10 mm. Finally, the cast thin sections after pressure perfusion and heating solidification were observed under a microscope, and the types of minerals, cements, and contact types in the rock were identified and analyzed.

2.5. Testing of Rock Mechanics Properties. The RMT-150C rock and concrete mechanics test system was used for the rock mechanics property test. A uniaxial compression test (natural water-bearing condition) was carried out on the samples to be tested according to the rock physical and mechanics properties test regulations (DZ/T 0276.18-2015). The test process was as follows: We processed samples into cylinders with a diameter of 60 mm and a height of 120 mm. The processed test piece (coated with a thin layer of vaseline lubricant on the upper and lower bottom surfaces) was placed in the center of the base. A rigid cushion block was placed between the upper end of the sample and the pressure bearing plate of the experimental machine. The pressure bearing head was adjusted so that the sample was uniformly stressed and loaded at a rate of 0.1−0.5 MPa/s until the sample was

https://doi.org/10.1021/acsomega.3c07731
ACS Omega 2024, 9, 1375−1388

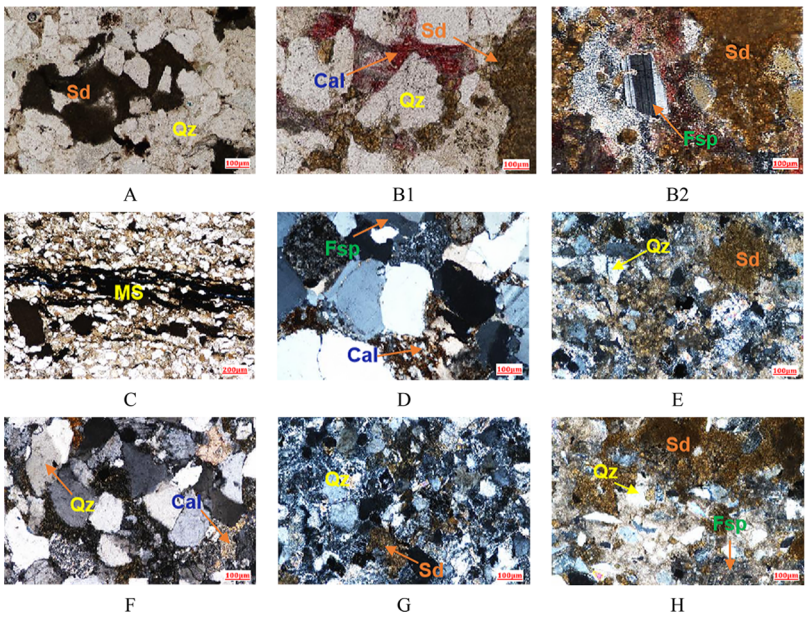

Figure 4. Cementation mode of minerals in the roof with different lithology. (A) Lithic quartz sandstone, ×10, MS sample. (B1) Siderite lithic quartz sandstone, ×10, FS-1 sample. (B2) Siderite lithic quartz sandstone, ×10, FS-2 sample. (C) Muddy siltstone, ×10, MS-1 sample. (D) Feldspathic lithic sandstone, ×10, FS-3 sample. (E) Feldspar lithic fine sandstone, ×10, MS-2 sample. (F) Lithic quartz sandstone, ×10, MS-3 sample. (G) Feldspathic lithic sandstone, ×10, FS-5 sample. (H) Feldspathic lithic sandstone, ×10, FS-6 sample. Sd, siderite; Qz, quartz; Cal, calcite; Fsp, feldspar; MS, muddy strip.

damaged. During the test, the specimen is placed at the center of the bearing plate of the press, and the bearing plate with a spherical seat is adjusted so that the specimen is uniformly loaded. The number of test specimens in each group shall not be less than 3 under the same water content state and the same loading direction. The display value error of the testing machine shall not exceed ±1%. Among them, soft rock and softer rock took a lower loading rate. According to the axial deformation and radial deformation of the rock specimen in the uniaxial compression test, the stress−strain curve of rock was drawn and the corresponding rock mechanics parameters were calculated.

3. RESULTS

In this study, experimental methods such as casting thin-section and X-ray whole rock analysis and mineral petrology analysis were carried out on sandstone of the roof and floor of the main coal seam in Xinxie-1 well (Figure 4 and Table 1), which mainly revealed the mineralogical composition, cementation type, and dissolving attack situation of rocks. The mineral composition of the rock at the roof and floor of the coal seam was dominated by quartz (average of 56.9%, with a range of 28−75.4%) and clay mineral (average of 30.4%, with a range of 11.2−64.3%), followed by anorthose (average of 6.0%, with a range of 0−23.6%), siderite (average of 5.1%, with a range of 0.4−43.3%), and pyrite (average of 0.4%, with a range of 0−3%); other minerals are scattered. The compressive strength (CS) of the roof and floor of each main coal seam was between 17.3 and 92.3 MPa, with an average of 52.01 MPa. The tensile strength (TS) was between 1.33 and 12.07 MPa, with an average of 4.73 MPa. The shear strength (SS) was between 5.3 and 18.5 MPa, with an average of 11.49 MPa. The softening coefficient (K) was between 0.15 and 0.83, with an average of 0.49. The modulus of elasticity (E) ranged from 5.36 to 28 GPa, with an average of 16.69 GPa. The Poisson's ratio (μ) is between 0.18 and 0.26, with an average of 0.22. The results of casting thin-section analysis were consistent with those in Table 1. It could be seen from Figure 3 that quartz, feldspar, and siderite were widely distributed in casting thin-section. The cementation types of the roof and floor of the coal seam were mainly quartz enlargement and siderite cementation (MS, FS-1, FS-2, MS-2, FS-5, and FS-6 samples), besides that argillaceous cementation and calcareous cementation were found in the roof of the local coal seam (MS-1, MS-3, and FS-3 samples). Except for a few feldspar and rock debris dissolved pores (Figure 4A), a few calcite metasomatic feldspar (Figure 4F) and organic matter strips (Figure 4C,H) were found. Quartz enlargement edges and siderite were common in the roof and floor of other coal seams, and no obvious dissolution was observed. In addition to the development of organic matter and fractures in the argillaceous zone, the whole rock was relatively dense with extremely poor porosity and permeability, and the pore damage caused by cementation was far greater than that caused by compaction.

4. DISCUSSION

4.1. Geological Occurrence Law of Mineral Compositions. *4.1.1. Mineral Distribution Law under Different Sedimentary Ages and Buried Depths.* With the increase of buried depth, the mineral content in the roof and floor of different coal seams showed different change rules. As shown in Figure 5, the measured data are fitted by a quadratic polynomial, so as to analyze the changing trend of mineral content with the change of buried depth.

It could be concluded that, with the increase of buried depth, the content of quartz in the roof and floor of the coal seam first decreased and then increased (Figure 5A), while the content of siderite first increased and then decreased (Figure 5B). Among them, the content of quartz was higher (>65%) in the roof of No. 13-1 and No. 4 coal seams and lower (<60%) in the roof and floor of No. 9 and No. 10 coal seams. The siderite content was opposite, but the inflection point was the

https://doi.org/10.1021/acsomega.3c07731
ACS Omega 2024, 9, 1375−1388

Table 1. List of Mineral Petrology and Rock Mechanics Parameters of the Roof and Floor of the Main Coal Seam

Sample number	Lithology	Stratum	Sampling depth/m	Rock composition/%							Rock mechanics parameters				
				Quartz	Plagioclase	Calcite	Ankerite	Siderite	Pyrite	Clay	CS/MPa	TS/MPa	SS/Mpa	K	E/GPa	μ
SM-1	sandy mudstone	roof of 13-1#	1149	47.00	0.80	0.00	0.00	2.30	0.00	49.90	26.00	1.33	5.50	0.330	7.00	0.25
SM-2	sandy mudstone	floor of 4-2#	1396	35.30	0.90	0.00	0.00	0.40	0.00	64.30	17.30	3.46	6.30	0.400	5.36	0.26
MS-1	muddy siltstone	floor of 12#	1162	58.40	0.70	0.00	0.00	4.60	0.00	36.30	41.1	3.29	9.0	0.640	11.00	0.22
MS-2	muddy siltstone	roof of 11-2#	1225	62.70	0.30	0.00	0.00	2.50	0.00	34.50	41.10	1.42	11.40	0.390	11.00	0.23
MS-3	muddy siltstone	floor of 8#	1304	60.00	5.10	0.00	0.00	3.20	0.00	31.70	27.00	3.63	5.30	0.190	7.00	0.24
MS-4	muddy siltstone	roof of 7#	1345	57.50	0.00	0.00	0.00	2.20	0.00	20.30	31.60	3.20	7.40	0.150	8.00	0.24
MS-5	muddy siltstone	roof of 4-2#	1390	67.80	10.80	0.00	0.00	0.80	1.20	29.40	29.50	5.18	14.30	0.710	10.00	0.23
SS	siltstone	roof of 9-3#	1289	67.30	6.70	0.00	0.00	2.50	0.00	23.50	78.00	4.54	8.80	0.760	22.00	0.20
FS-1	fine sandstone	roof of 13-1#	1146	28.00	1.40	9.50	6.60	43.30	0.00	11.20	86.40	12.07	18.20	0.750	28.00	0.18
FS-2	fine sandstone	roof of 10#	1266	58.30	23.60	0.00	0.00	4.70	0.30	13.00	58.5	3.70	16.2	0.830	19.00	0.21
FS-3	fine sandstone	roof of 9-3#	1283	68.00	2.60	1.50	0.00	3.30	0.80	23.80	51.8	11.10	7.3	0.490	16.00	0.22
FS-4	fine sandstone	floor of 9-3#	1296	57.80	10.80	0.00	0.00	0.80	1.20	29.40	69.8	4.80	18.5	0.510	23.00	0.18
FS-5	fine sandstone	roof of 9-2#	1299	58.60	12.70	0.00	0.00	3.30	3.00	22.30	75.50	6.09	16.30	0.360	24.00	0.19
FS-6	fine sandstone	roof of 8#	1338	61.40	7.00	0.00	0.00	1.70	0.00	29.90	54.20	4.00	17.50	0.450	18.00	0.22
MS	medium sandstone	roof of 13-1#	1137	75.40	7.00	0.70	0.00	0.40	0.00	16.50	92.30	2.43	10.40	0.440	26.00	0.19

same, which was located at the bottom of the Upper Shihezi Formation and the top of the Lower Shihezi Formation. The analysis might be related to the development of interbedded sandstone and mudstone in the transitional zone of the delta plain.[39] In addition, with the increase of buried depth, the content of plagioclase and clay minerals in the roof and floor of the coal seam changed gradually. Among them, the content of plagioclase approximately increased with the increase of buried depth (Figure 5C), while the content of clay minerals approximately decreased with the increase of buried depth (Figure 5D).

Different rocks have different types, contents, and combinations of minerals, as well as the content of elements contained in each mineral. In addition, the duration of the transportation distance affects the morphology and structure of the rocks. Figure 5 indicates the lithology, composition, particle size, sedimentary structure, sorting, and rounding information on the roof of the main mining coal seam of the Early Permian coal-bearing series in this study area, which provides petrographic evidence for further understanding of the sedimentary environments of the rock strata. It has been demonstrated that the Huainan area experienced a seawater oscillatory retreat event during the Early Permian period, and the sedimentation was generally submerged.[40] Quartz was mostly dominant in the clastic composition of this sedimentary system, and siderite was a common occurrence in riparian avalanches. The lithological composition of the sedimentary environment of the Lower Shihezi Formation was composed of predominantly deltaic plain sedimentary development, which belongs to the transition zone between the Upper and Lower deltaic plains. The sedimentary environment of the Upper Shihezi Formation was developed over a long period of time to form a broader delta plain. Therefore, it is believed that the changes in the sedimentary cyclones of the Lower and Upper Shihezi Formations played a certain role in controlling the formation of minerals in the sedimentary clastic rocks.

4.1.2. Mineral Distribution Law under Different Lithologic Conditions. The mechanical behavior of rock at the macroscale depended largely on its granular mesoscale structure and the properties of each mineral composition.[41] It could be seen from Figure 6 that the mineral content changed regularly under different roof and floor conditions of coal seam lithology conditions. The concrete manifestations were as follows: (1) The change trend of quartz and clay minerals in the roof and floor of the coal seam was the most obvious, followed by plagioclase and siderite (Figure 6). (2) With the increase of rock particle size (i.e., sandy mudstone < argillaceous siltstone < siltstone < fine sandstone < medium sandstone), the content of quartz and plagioclase minerals gradually increased (Figure 6A and B). The content of siderite changed relatively little, showing a gradual increase trend (Figure 6C), whereas the content of clay decreased gradually (Figure 6D).

It could be seen that the larger the particle size of rock (such as medium sandstone and fine sandstone), the higher the content of quartz and plagioclase in rock and the lower the content of clay. On the contrary, the smaller the particle size of rock (such as sandy mudstone and argillaceous siltstone), the lower the content of quartz and plagioclase and the higher the content of clay. Under different lithologic conditions, the content of siderite did not change obviously but local aggregation easily occurred in fine sandstone and medium sandstone formations. The content of siderite varies insignificantly under different lithological conditions (different particle

https://doi.org/10.1021/acsomega.3c07731
ACS Omega 2024, 9, 1375−1388

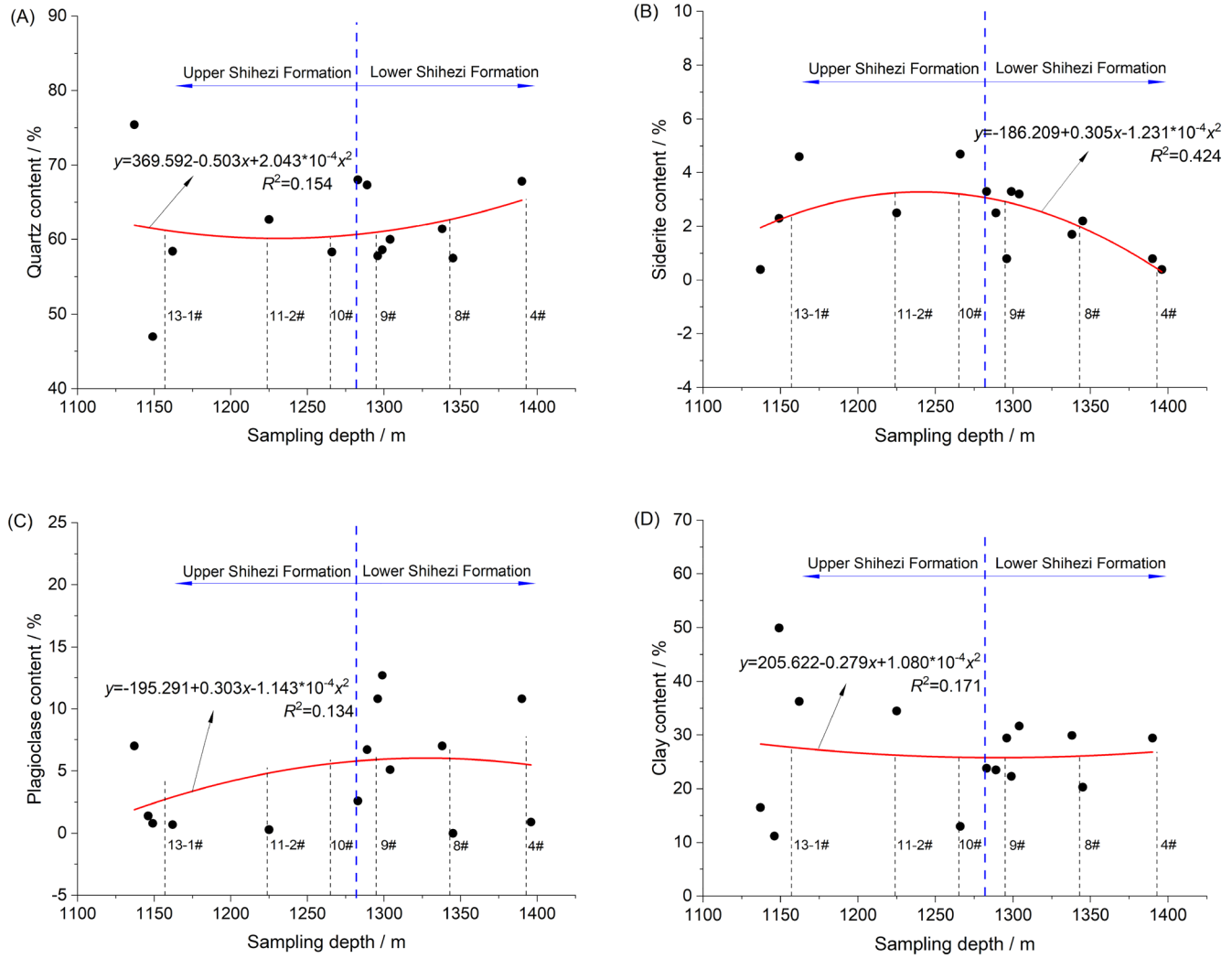

Figure 5. Variation of the contents of four minerals (quartz (A), siderite (B), plagioclase (C), and clay (D)) with sampling depth.

sizes of clasts), but it occurs as a partial occurrence of accumulation in fine sandstones and muddy siltstones. In general, siderite was formed in a slightly reduced−oxidized environment.[42,43] This coincides with the petrographic characteristics of the Lower-Upper Shihezi Formations. The postgeneration interaction was the most significant diagenetic type for the formation of siderite in fine sandstones and muddy siltstones.[44] For sandy siltstone with a small clastic particle size, siderite may be a product of early diagenesis.

4.2. The Relationship between Mineral Composition and Rock Mechanics Properties of Coal Seam Roof and Floor. In conventional reservoir fracturing design, mechanics parameters such as the elastic modulus (E), Poisson's ratio (μ), and compressive strength (CS) of rocks were often used to predict the fracturability and fracture pressure of reservoir rocks, and petrological characteristics were the most important factors affecting the mechanics properties of rocks.[7,45,46] When the content of mineral compositions in rocks was different, the mechanical properties of rocks must be different. With the change of lithologic composition, the rock mechanics properties of the roof and floor of coal seams showed different laws (Figure 7A and B). It showed as follows: (1) With the increase of rock particle size, the two parameters (CS and E) showed an increasing trend. It was characterized by sandy mudstone < argillaceous siltstone < siltstone < fine sandstone < medium sandstone. Poisson's ratio (μ) showed a decreasing trend, and other rock mechanics parameters did not change obviously. The above conclusions were consistent with:[23] (2) In general, quartz, feldspar, and clay mainly affected the elastic modulus of shale. The increase of quartz and feldspar content led to the increase of elastic modulus, while clay minerals had the opposite. On the contrary, carbonate and organic matter had little effect on the elastic modulus of rock,[23] which was slightly different from this study. In comparison to the shear strength (SS), softening coefficiency (K), and μ, the increase of siderite content was an important factor causing an abnormal increase of CS, tensile strength (TS), and E values of rocks. For example, the content of siderite in the FS-2 sample was 43%, which corresponded to the CS, TS, and E values of this sample being 86.4 MPa, 12.07 MPa, and 28 GPa, respectively. Therefore, the influence of the change of carbonate content on rock mechanics properties in the study area needed to be paid attention to: (3) Under the same rock composition condition, the different rock particle cementation methods would lead to significant differences in rock mechanics parameters.[47] For example, the whole rock analysis results of the MS-2 and MS-3 samples were relatively similar. The content of quartz was between 60 and 63%, and the content of siderite was between 2 and 3%. According to the previous analysis, the siderite cementation of the MS-2 sample was relatively developed,

https://doi.org/10.1021/acsomega.3c07731
ACS Omega 2024, 9, 1375−1388

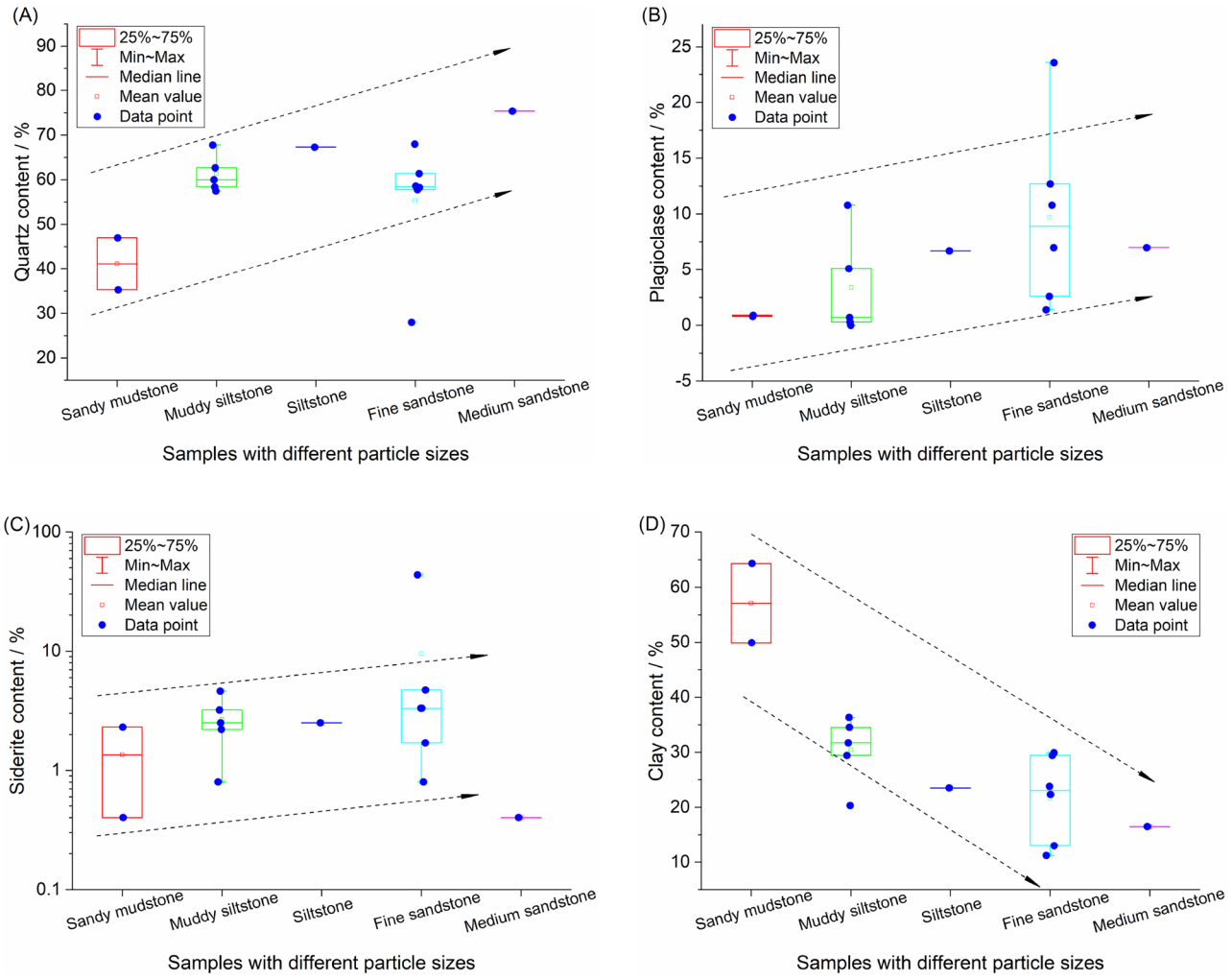

Figure 6. Variation of four mineral contents (quartz (A), plagioclase (B), siderite (C), and clay (D)) as a function of the particle size.

while the cementing method of the MS-3 sample was mainly siliceous cement. The difference in the type of cementation might be an important reason for the obvious difference in the CS, SS, and E values of the MS-2 samples.[47,48] (4) According to the physical meaning of brittleness in elastic mechanics, more generally, the larger the E, the smaller the μ, which was consistent with the change law of E and μ in Figure 7B. It could be preliminarily speculated that fine sandstone and medium sandstone with a large particle size of rock particles had good compressive strength, tensile strength, shear strength, elastic modulus, and brittleness characteristics. However, in view of the differences in mineral composition and cementation type, there would be different degrees of impact on the mechanics properties and brittleness characteristics of rocks. Therefore, the effective and reasonable determination of the weight coefficients of different rock minerals was the key to quantitatively evaluate the mechanical characteristics and brittleness characteristics of rocks.

4.3. Contribution of Mineral Compositions to Rock Mechanics Properties of Coal Seam Roof and Floor. *4.3.1. An Overview of Gray Correlation Model.* Different mineral components contributed differently to the mechanics properties of rocks.[49−53] In order to quantitatively evaluate the contribution of mineral groups to the mechanics properties of coal seam roof rock and simplify the model parameters, the influences of minerals such as ankerite, pyrite, and calcite were not considered for the time being.[54] When considering the contribution of mineral composition to the mechanics properties of coal roof and floor rocks, due to the incompleteness and uncertainty of the understanding of internal mineral composition, the influence of various factors on the mechanics properties cannot be determined at once, which requires in-depth research. The gray correlation analysis method makes up for the deficiency of using the mathematical statistics method for system analysis. It is equally applicable to the number of samples and the regularity of samples; the calculation is small, which is very convenient, and there will be no discrepancy between quantitative and qualitative analysis results. In this paper, the gray correlation analysis method is proposed.[55]

4.3.2. Preprocessing of the Initial Sequence. Due to the different magnitude of each impact parameter, it is necessary to carry out dimensionless processing in the gray correlation analysis. This paper adopts the great value standardization method, which is different according to the significance of the parameter, and the processing method is also different, which is mainly divided into two cases: for the positive indicator, that is, the impact factor is positively correlated with the rock brittleness, dividing the single parameter data by the maximum value of this indicator; for the negative indicator, first

https://doi.org/10.1021/acsomega.3c07731
ACS Omega 2024, 9, 1375−1388

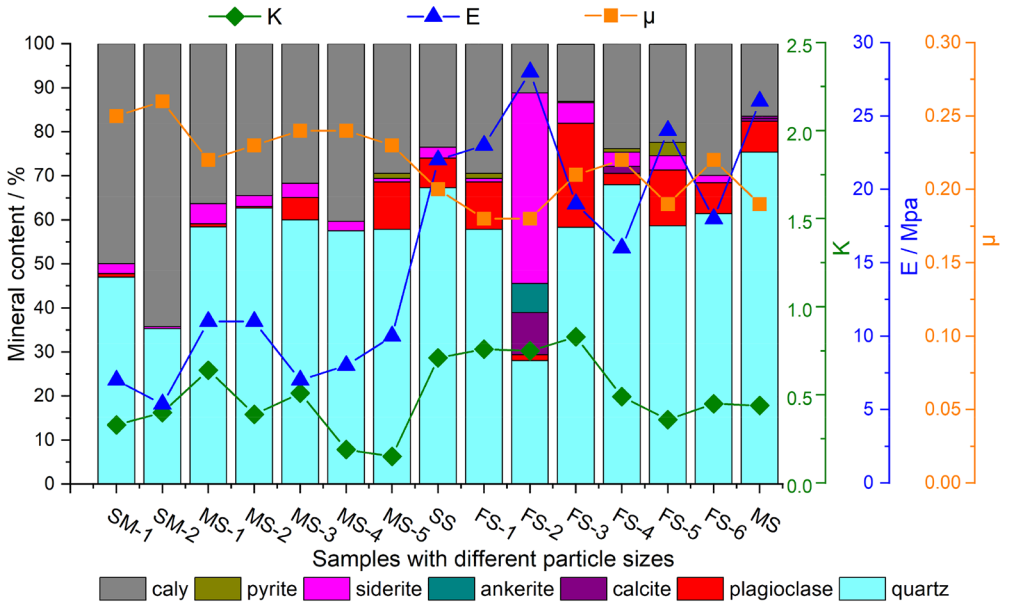

(A)

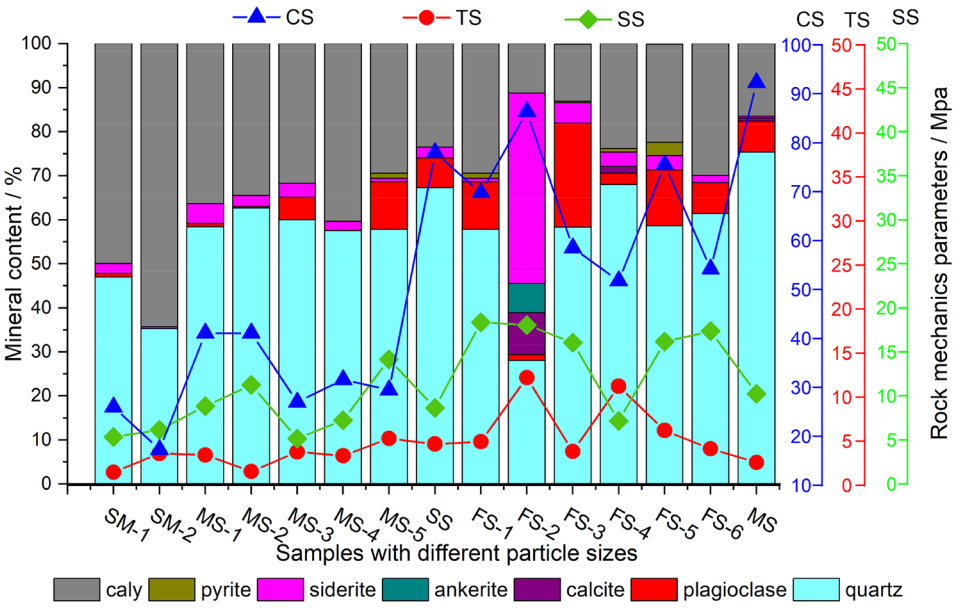

(B)

Figure 7. (A) Variation of mineral content and rock mechanics parameters (CS, TS, and SS) in samples with different particle sizes. (B) Variation of mineral content and rock mechanics parameters (K, E, and μ) in samples with different particle sizes.

subtracting the single parameter data from the great value of this parameter and then dividing the great value by the difference of the parameter.

4.3.3. Determining the Parent Sequence. Rock mineral composition (quartz, plagioclase, siderite, and clay) and mechanics parameters (CS, TS, SS, K, E, and μ) were selected as subindicators and parent indicators, respectively. According to the basic principles of the gray correlation model, computer programming was carried out using the MATLAB language. The contribution of each mineral content to the mechanical properties of the rock was quantitatively calculated in accordance with the output results.

4.3.4. Calculation of the Gray Correlation Coefficient. Let $\xi_i(K)$ $(i = 1, 2, ..., m)$ be the correlation coefficient of x_i to x_0 at the sampling position of K; then,

$$\xi_i(K) = \frac{\Delta_{\min} + k\Delta_{\max}}{\Delta_i(K) + k\Delta_{\max}} \quad (1)$$

where K was the resolution coefficient (the value was between $[0.1, 1]$, generally 0.5); $\Delta_{\min}$ is the minimum absolute value

https://doi.org/10.1021/acsomega.3c07731
ACS Omega 2024, 9, 1375−1388

Table 2. Normalized Results of Each Evaluation Index and Brittleness Index

	Subindicator				Parent indicator					
Sample number	Quartz	Plagioclase	Siderite	Clay	CS	TS	SS	K	E	μ
SM-1	0.62	0.03	0.05	0.78	0.28	0.11	0.30	0.40	0.25	0.96
SM-2	0.47	0.00	0.01	1.00	0.19	0.29	0.34	0.48	0.19	1.00
MS-1	0.77	0.03	0.11	0.56	0.45	0.27	0.49	0.77	0.39	0.85
MS-2	0.83	0.01	0.06	0.54	0.45	0.12	0.62	0.47	0.39	0.88
MS-3	0.80	0.22	0.07	0.49	0.29	0.30	0.29	0.23	0.25	0.92
MS-4	0.76	0.00	0.05	0.63	0.34	0.27	0.40	0.18	0.29	0.92
MS-5	0.77	0.46	0.02	0.46	0.32	0.43	0.77	0.86	0.36	0.88
SS	0.89	0.28	0.06	0.37	0.85	0.38	0.48	0.92	0.79	0.77
FS-1	0.77	0.46	0.02	0.46	0.94	1.00	0.98	0.90	1.00	0.69
FS-2	0.37	0.06	1.00	0.17	0.63	0.31	0.88	1.00	0.68	0.81
FS-3	0.77	1.00	0.11	0.20	0.56	0.92	0.39	0.59	0.57	0.85
FS-4	0.90	0.11	0.08	0.37	0.76	0.40	1.00	0.61	0.82	0.69
FS-5	0.78	0.54	0.08	0.35	0.82	0.50	0.88	0.43	0.86	0.73
FS-6	0.81	0.30	0.04	0.47	0.59	0.33	0.95	0.54	0.64	0.85
MS	1.00	0.30	0.01	0.26	1.00	0.20	0.56	0.53	0.93	0.73

difference, $\Delta_{\min} = \min_i \min_K |x_0(K) - x_i(K)|$ (generally, 0 is acceptable); $\Delta_{\max}$ is the maximum absolute value difference, $\Delta_{\max} = \max_i \max_K |x_0(K) - x_i(K)|$; $\Delta_i(K)$ is the absolute difference between the factors at the sampling point K, $\Delta_i(K) = |x_0(K) - x_i(K)|$.

4.3.5. Calculation of the Correlation Degree. The information represented by individual correlation coefficients is scattered and not comparable. For comparison purposes, the correlation degree of x_i to x_0 was adopted to centralize them

$$\gamma_i = \frac{1}{N}\sum_{i=1}^{n} \xi_i(K) \tag{2}$$

where γ_i is the correlation degree of the subindicator relative to the parent indicator.

4.3.6. Determination of Weight Coefficients. After the correlation degree of each evaluation index was calculated, the weight coefficient of each evaluation index could be obtained by normalization. The normalized equation was expressed as

$$a_i = \frac{\gamma_i}{\sum_{i=1}^{m} \gamma_i} \tag{3}$$

where a_i is the weight coefficient and m is the number of evaluation indexes.

The normalized results are listed in Table 2, and the results of weight coefficient calculations are presented in Table 3 and Figure 8.

It could be seen from Figure 8 that the weight coefficients of different mineral compositions corresponding to rock mechanics parameters were also different, which was shown

Table 3. Weight Coefficient of Each Evaluation Index

	Weight coefficient			
Parent indicator	Quartz	Plagioclase	Siderite	Clay mineral
CS	0.2799	0.2431	0.2281	0.2489
TS	0.2058	0.2785	0.2578	0.2579
SS	0.2743	0.2461	0.222	0.2576
K	0.2768	0.2557	0.2141	0.2533
E	0.2722	0.2557	0.2142	0.2533
μ	0.3471	0.2116	0.1777	0.2637

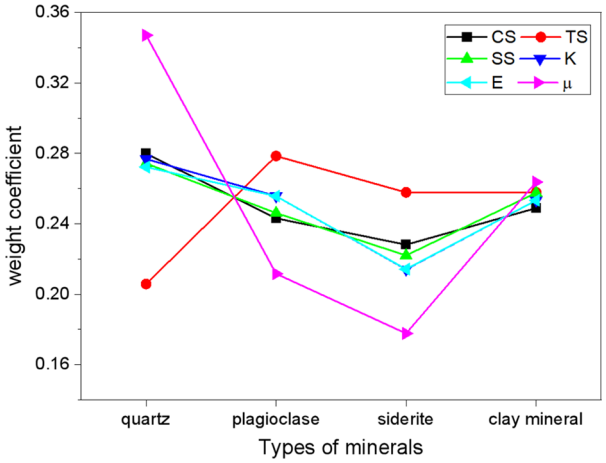

Figure 8. Weight coefficients of different mineral compositions corresponding to rock mechanics parameters.

as follows: (1) quartz minerals had the largest contribution to the Poisson's ratio (0.3471) and the smallest contribution to the tensile strength (0.2058), and the contribution to other rock mechanics parameters was about 0.28. (2) Oblique feldspar and siderite had the same contribution to the above six rock mechanics parameters, which generally showed that they had a greater contribution to tensile strength, a smaller contribution to Poisson's ratio, and a general contribution to other rock mechanics parameters. (3) The influence of clay minerals on rock mechanics parameters was consistent, and each weight coefficient was approximately 0.25. Therefore, the variations in the content of brittle minerals such as quartz, plagioclase feldspar, and rhodochrosite in the rocks are more sensitive to the mechanics properties of the rocks when compared to clay minerals. It is quartz that is more sensitive to compressive strength, shear strength, modulus of elasticity, softening coefficient, and Poisson's ratio, plagioclase and siderite to tensile strength, and clay minerals to Poisson's ratio. The above results were basically consistent with the conclusion of Liu et al.[23] It should be pointed out that clay content had a direct impact on Poisson's ratio, which was positively correlated with Poisson's ratio, while quartz content was inversely related to Poisson's ratio.

https://doi.org/10.1021/acsomega.3c07731
ACS Omega 2024, 9, 1375−1388

4.4. Evaluation Method of Brittleness of the Coal Seam Top and Bottom Plates Based on Mineral Composition. At present, Li et al.[54] had tried to establish a brittleness evaluation method based on rock mineral composition and mechanics parameters, but the model lacked universal applicability due to the influence of evaluation index selection. Therefore, in the brittleness evaluation, the mineral composition (quartz, plagioclase, siderite, and clay) and mechanics parameters (E and μ) of the rock in the study area were comprehensively considered as the key indicators for the evaluation of rock brittleness, and a new method for evaluating the rock brittleness—mineral weight analysis method was proposed. This time, the rock brittleness ($BIavg$) determined by the elastic parameter method was taken as the parent indicator, and the specific calculation method of the parent indicator was as follows:

$$E\_BI = (E\_C - E\_min)/(E\_max - E\_min) \quad (4)$$

$$\mu\_BI = (\mu\_C - \mu\_max)/(\mu\_min - \mu\_max) \quad (5)$$

$$BI_{avg} = (E\_BI + \mu\_BI)/2 \quad (6)$$

E_C and μ_C are the calculated elastic modulus and Poisson's ratio; E_max and E_min are the maximum and minimum of elastic modulus; μ_max and μ_min are the maximum and minimum Poisson's ratio; E_BI and μ_BI are the brittleness of rock calculated for the elastic modulus and Poisson's ratio, respectively; and BI_{avg} is the average value of rock brittleness. Since the measured sample data were few, the values of maximum and minimum values of the elastic modulus and Poisson's ratio refer to Rickman et al.[25] According to Rickman et al.,[25] under the condition of large sample data, E_max = 85 MPa, E_min = 5 MPa, μ_max = 0.37, and μ_min = 0.16. The main mineral compositions (quartz, plagioclase, siderite, and clay minerals) of the roof and floor of the coal seam were adopted as the classification indexes, and the weight coefficient of each mineral composition on the brittleness index was determined using the gray correlation analysis method. After calculation, the weight coefficients of quartz, plagioclase, siderite, and clay minerals were 0.3271,0.2244, 0.1919, and 0.2566, respectively. In order to highlight more brittle rocks, the author put forward a new formula for calculating the brittleness (BI) of rocks in this area:

$$\begin{aligned} \mathrm{BI} = {} & [(V_{\mathrm{Quartz}} \times 0.3271) + (V_{\mathrm{Carbonatite}} \times 0.1919)] \\ & /[(V_{\mathrm{Quartz}} \times 0.3271) + (V_{\mathrm{Plagioglase}} \times 0.2244) \\ & + (V_{\mathrm{Carbonatite}} \times 0.1919) + (V_{\mathrm{Clay}} \times 0.2566)] \end{aligned} \quad (7)$$

In order to verify the rationality of the above formula, the calculation results were compared with the rock mechanics parameter method and the rock mineralogy method (Figure 9).

It could be seen from Figure 9 that the calculation result of the rock mechanics parameter method was low, which was related to the lack of consideration of rock mineral composition in this method.[38] Although the results of the rock mineralogy method were close to the results calculated by the mineral weight analysis method, the comprehensive influence of brittle minerals in carbonate rocks on the brittleness index was not considered. When the content of calcite, siderite, and other carbonate minerals in rocks was abnormal, the calculated results would be abnormal (FS-2 sample in Figure 9). The new formula proposed by the author considered the influence of carbonate minerals widely existing in the study area, and the calculated results were more realistic and could avoid the occurrence of abnormal data results.

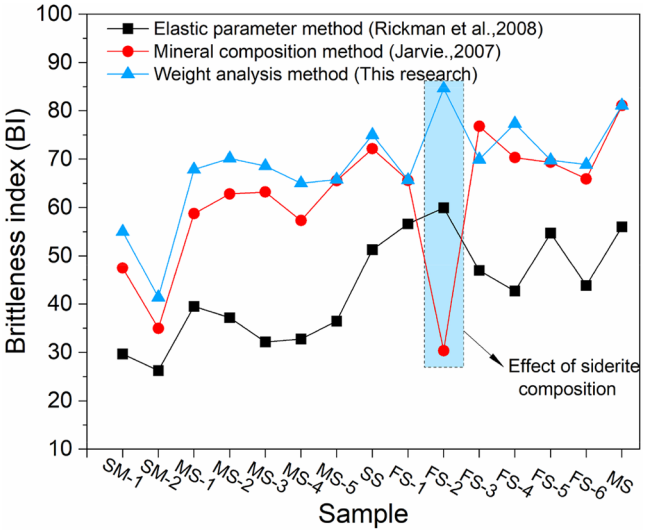

Figure 9. Comparison of different calculation methods of the brittleness index.

Figure 10 shows the evaluation results of the brittleness of the roof and floor of different coal seams obtained by using the

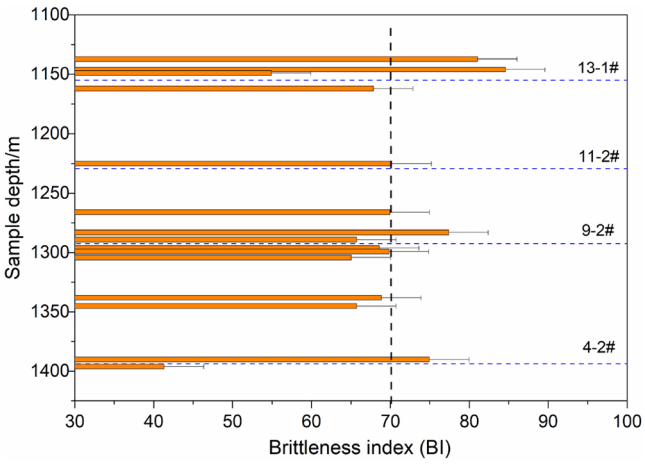

Figure 10. Brittleness evaluation of the roof and floor of different coal seams.

new calculation formula. With the increase of buried depth of the coal seam, the brittleness coefficient of the roof and floor of the coal seam in Xinxie-1 well generally showed a decreasing trend. In this study, the rock samples showed typical brittle damage after uniaxial compression tests. That is, the sandstone showed a strong brittle fracture when compressed, and when the load reached the maximum, the stress suddenly experienced a drop phenomenon. In the uniaxial compression test, the damage mode of samples with high brittleness index is dominated by shear damage, with fewer cracks after damage; the damage mode of samples with lower brittleness index undergoes tensile damage, with more cracks after damage in general. In addition, the time of occurrence of brittle fracture varies among rock samples with different lithologies.[56,57] The roof and floor of coal seams with a brittleness coefficient

https://doi.org/10.1021/acsomega.3c07731
ACS Omega 2024, 9, 1375−1388

greater than 70 were mainly the roof of 13-1, 11-2, 9-2, and 4-2 coal seams. The above-mentioned coal seam roof tends to form a fracture network, which had guiding significance for the optimization of fracturing horizon.

5. CONCLUSIONS

In this paper, the mineral composition and brittleness characteristics of the rocks on the roof and floor of the main mining coal seam in Xinxie-1 well of the Huainan Coalfield, Anhui Province, China, are investigated. The following main conclusions are obtained from the in-depth analysis of the rock samples:

(1) Mineral contents in the rocks at the roof and floor of the coal seam show different variation characteristics as a function of the depth and lithology. The differences in the mineral composition and cementation type of the rocks are the essential factors that lead to their different rock mechanics properties.

(2) In contrast to clay minerals, the changes in the content of brittle minerals such as quartz, plagioclase, and siderite in rocks are relatively sensitive to the mechanics properties of the rocks.

(3) The evaluation method of rock brittleness of the roof and floor of the coal seam was constructed based on the mineral weight analysis, and the calculation results show that the rock brittleness indexes of the roof of the 13-1, 11-2, 9-2, and 4-2 coal seams are larger, reflecting the higher fracture extension pressure of the rock, which is favorable for the formation of a fracturing network.

AUTHOR INFORMATION

Corresponding Authors

Jian Wu − *AnHui Provincial Key Laboratory of Intelligent Underground Detection, College of Civil Engineering, Anhui Jianzhu University, Hefei, Anhui 230601, China;* orcid.org/0000-0003-4654-775X; Phone: 18155922108; Email: wj18155922108@163.com; Fax: +86-0551-65846101

Guangqing Hu − *Green Mining Engineering Technology Research Center of Anhui Province, Exploration Research Institute, Anhui Provincial Bureau of Coal Geology, Hefei 230088, China*; Phone: 18155922108; Email: huguangqing117@163.com; Fax: +86-0551-65846101

Authors

Dun Wu − *AnHui Provincial Key Laboratory of Intelligent Underground Detection, College of Civil Engineering, Anhui Jianzhu University, Hefei, Anhui 230601, China; School of Earth and Space Sciences, University of Science and Technology of China, Hefei 230026, China;* orcid.org/0000-0002-4906-8263

Bo Li − *AnHui Provincial Key Laboratory of Intelligent Underground Detection, College of Civil Engineering, Anhui Jianzhu University, Hefei, Anhui 230601, China*

Xia Gao − *School of Architecture & Urban Planning, Anhui Jianzhu University, Hefei, Anhui 230601, China*

Jianwei Lu − *AnHui Provincial Key Laboratory of Intelligent Underground Detection, College of Civil Engineering, Anhui Jianzhu University, Hefei, Anhui 230601, China*

Complete contact information is available at: https://pubs.acs.org/10.1021/acsomega.3c07731

Author Contributions

Dun Wu and Bo Li: conceptualization and writing, original draft preparation. Jian Wu and Guangqing Hu: methodology. Dun Wu and Bo Li: investigation. Xia Gao and Jianwei Lu: software. Jian Wu, Guangqing Hu, and Xia Gao: writing, review, and editing. The manuscript was written through contributions of all authors. All authors have given approval to the final version of the manuscript.

Funding

We would like to extend our sincere gratitude to the Anhui Jianzhu University Introduction of Talents and Doctoral Initiation Fund Project (2022QDZ22), the Open Fund Project of Anhui Green Mine Engineering Research Center (2022KJ03), the Anhui Province Key Research and Development Program Projects (2022n07020005), and the Academic Funding Program for Top Talents in Higher Education Disciplines (gxbjZD2022145).

Notes

The authors declare no competing financial interest.

ACKNOWLEDGMENTS

We thank the staff at the Key Laboratory of Intelligent Underground Detection Technology for Anhui Jianzhu University for support.

NOMENCLATURE

CS	compressive strength
TS	tensile strength
SS	shear strength
K	softening coefficient
E	modulus of elasticity
μ	Poisson's ratio
Sd	siderite
BI	brittleness index

REFERENCES

(1) Dai, J.; Gong, D.; Ni, Y.; Huang, S.; Wu, W. Stable carbon isotopes of coal-derived gases sourced from the Mesozoic coal measures in China. *Org. Geochem.* **2014**, *74*, 123−142.

(2) Zhu, Y.; Hou, X.; Cui, Z.; Liu, G. Resources and reservoir formation of unconventional gas in coal measure, Hebei Province. *Journal of China Coal Society* **2016**, *41*, 202−211.

(3) Wu, D.; Zhang, W.; Liu, G.; Zhan, R.; Hu, G. Characteristics and geological significance of germanium in Taiyuan coal formation of Huainan Coalfield, Anhui, China. *Int. J. Coal. Sci. Techn.* **2020**, *7*, 662−675.

(4) Yuan, L.; Xue, J.; Zhang, N.; Lv, P. Development orientation and status of key technology for mine underground coal bed methane drainage as well as coal and gas simultaneous mining. *Coal Science and Technology* **2013**, *41*, 6−11.

(5) Zhang, Q.; Ge, C.; Li, W.; Jiang, Z.; Chen, J.; Li, B.; Wu, J.; Wu, X.; Liu, J. A new model and and application of coalbed methane high efficiency production from broken soft and low permeable coal seam by roof strata-in horizontal well and staged hydraulic fracture. *Journal of China Coal Society* **2018**, *43*, 150−159.

(6) Wu, X.; Zhang, Q. Research on controlling mechanism of fracture propagation of multi-stage hydraulic fracturing horizontal well in roof of broken soft and low permeability coal seam. *Nat. Gas. Geosci.* **2018**, *29*, 12.

(7) Wu, Q.; Xu, Y.; Wang, X.; Wang, T.; Zhang, S. Volume fracturing technology of unconventional reservoirs: connotation, design optimization and implementation. *Petrol. Explor. Dev.* **2012**, *39*, 377−384.

(8) Rahimzadeh Kivi, I.; Ameri, M.; Molladavoodi, H. Shale brittleness evaluation based on energy balance analysis of stress-strain curve. *J. Petrol. Sci. Eng.* **2018**, *167*, 1−19.
(9) Raef, A. E.; Kamari, A.; Totten, M.; Harris, D.; Johnson, K.; Lambert, M. The dynamic elastic and mineralogical brittleness of woodford shale of the anadarko basin: ultrasonic p-wave and s-wave velocities, XRD-mineralogy and predictive models. *J. Petrol. Sci. Eng.* **2018**, *169*, 33−43.
(10) Ward, C. R. Analysis and significance of mineral matter in coal seam. *Int. J. Coal Geol.* **2002**, *50*, 135−168.
(11) Dai, S.; Ren, D.; Hou, X.; Shao, L. Geochemical and mineralogical anomalies of the late Permian coal in the Zhijin coalfield of southwest China and their volcanic origin. *Int. J. Coal Geol.* **2003**, *55*, 117−138.
(12) Dai, S.; Ren, D.; Zhou, Y.; Chou, C.; Wang, X.; Zhao, L.; Zhu, X. Mineralogy and geochemistry of a superhigh-organic-sulfur coal, Yanshan Coalfield, Yunnan, China: Evidence for a volcanic ash component and influence by submarine exhalation. *Chem. Geol.* **2008**, *255*, 182−194.
(13) Jarvie, D. M.; Hill, R. J.; Ruble, T. E.; Pollastro, R. M. Unconventional shale-gas systems: The Mississippian Barnett Shale of north-central Texas as one model for thermogenic shale-gas assessment. *AAPG Bull.* **2007**, *91*, 475−499.
(14) Zhang, C.; Dong, D.; Wang, Y.; Guan, Q. Brittleness evaluation of the Upper Ordovician Wufeng−Lower Silurian Longmaxi shale in Southern Sichuan Basin, China. *Energy Explor. Exploit.* **2017**, *35*, 430−443.
(15) Mbenoun, M. A.; Ngon Ngon, G. F.; Ngouabe, G. T.; Mbog, M. B.; Mbaï, J. S.; Bilong, P. Mineralogical and geochemical characterization of weathered materials in the gold-bearing quartz veins, Mintom area, Southern Cameroon. *Arab. J. Geosci.* **2023**, *16*, 105.
(16) Li, X.; Cao, S.; Zhou, D.; Liu, J.; Jiang, S.; Li, W.; Cheng, X.; Bai, J.; Wu, Y. Deformation and mineralizing fluid circulation of gold-silver-bearing quartz veins in the Yushishan gold deposit, Altyn Mountain, northwestern China. *Ore. Geol. Rev.* **2023**, *154*, No. 105339.
(17) Oye, O. J.; Aplin, A. C.; Orland, I. J.; Valley, J. W. Low volumes of quartz cement in deeply buried Fulmar Formation sandstones explained by a low effective stress burial history. *Geo. Sci. Eng.* **2023**, *221*, No. 211383.
(18) Walderhaug, O. Kinetic Modeling of Quartz Cementation and Porosity Loss in Deeply Buried Sandstone Reservoirs. *AAPG Bull.* **1996**, *80*, 731−745.
(19) Railsback, L. B. Carbonate diagenetic facies in the Upper Pennsylvanian Dennis Formation in Iowa, Missouri, and Kansas. *J. Sediment. Res.* **1984**, *54*, 986−999.
(20) Zou, C. N.; Tao, S. Z.; Zhou, H.; Zhang, X. X.; He, D. B.; Zhou, C. M.; Wang, L.; Wang, X. S.; Li, F. H.; Zhu, R. K.; Luo, P.; Yuan, X. J.; Xu, C. C.; Yang, H. Genesis, classification and evaluation method of diagenetic facies. *Petrol. Explor. Dev.* **2008**, *35*, 526−540.
(21) Li, Y.; Jia, D.; Rui, Z.; Peng, J.; Fu, C.; Zhang, J. Evaluation method of rock brittleness based on statistical constitutive relations for rock damage. *J. Petrol. Sci. Eng.* **2017**, *153*, 123−132.
(22) Kim, T.; Hwang, S. Petrophysical approach for S-wave velocity prediction based on brittleness index and total organic carbon of shale gas reservoir:a case study from Horn River Basin, Canada. *J. Appl. Geophys.* **2017**, *136*, 513−520.
(23) Liu, B.; Wang, S.; Ke, X.; Fu, X.; Pan, Z. Mechanical characteristics and factors controlling brittleness of organic-rich continental shales. *J. Petrol. Sci. Eng.* **2020**, *194*, 107464.
(24) Josh, M.; Esteban, L.; Delle Piane, C.; Sarout, J.; Dewhurst, D. N.; Clennell, M. B. Laboratory characterisation of shale properties. *J. Petrol. Sci. Eng.* **2012**, *88*, 107−124.
(25) Rickman, R.; Mullen, M. J.; Petre, J. E.; Grieser, W. V.; Kundert, D. A Practical Use of Shale Petrophysics for Stimulation Design Optimization: All Shale Plays Are Not Clones of the Barnett Shale. *Paper presented at the SPE Annual Technical Conference and Exhibition, Denver, Colorado, USA*. 2008, SPE-115258-MS.
(26) Tarasov, B.; Potvin, Y. Universal criteria for rock brittleness estimation under triaxial compression. *Int. J. Rock. Mech. Min.* **2013**, *59*, 57−63.
(27) Li, H. Research progress on evaluation methods and factors influencing shale brittleness: A review. *Energy*. **2022**, *8*, 4344−4358.
(28) Ai, C.; Zhang, J.; Li, Y. W.; Zeng, J.; Yang, X. L.; Wang, J. G. Estimation Criteria for Rock Brittleness Based on Energy Analysis During the Rupturing Process. *Rock. Mech. Rock.* **2016**, *49*, 4681−4698.
(29) Fan, M.; Jin, Y.; Chen, M.; Geng, Z. Mechanical characterization of shale through instrumented indentation test. *J. Petrol. Sci.* **2019**, *174*, 607−616.
(30) Zhou, H.; Chen, J.; Lu, J. J.; Jiang, Y.; Meng, F. Z. A New Rock Brittleness Evaluation Index Based on the Internal Friction Angle and Class I Stress-Strain Curve. *Rock, Mech. Rock.* **2018**, *51*, 2309−2316.
(31) Yin, X. Y.; Liu, X. J.; Zong, Z. Y. Pre-stack basis pursuit seismic inversion for brittleness of shale. *Petro. Sci.* **2015**, *12*, 618−627.
(32) Sui, L. L.; Ju, Y.; Yang, Y. M.; Yang, Y.; Li, A. S. A quantification method for shale fracability based on analytic hierarchy process. *Energy*. **2016**, *115*, 637−645.
(33) Wang, F. P.; Gale, J. F. W. Screening criteria for shale-gas system. *Gulf Coast Association of Geological Societies Transactions.* **2009**, *59*, 779−793.
(34) Jin, X. C.; Shan, S. N.; Roegiers, J. C.; Zhang, B. Fracability evaluation in shale reservoirs-An integrated petrophysics and geomechanics approach. *SPE J.* **2014**, *20*, 518−526.
(35) Sun, S. S.; Rui, Y.; Shi, Z. S.; Wu, J.; Ma, C. Application of a lithofacies model to characterise the gas shale in the Wufeng and Lungmachi formations, NE Sichuan Basin, China. *Appl.Earth.Sci.* **2018**, *127*, 115−122.
(36) Singh, S.; Qiu, F. M.; Morgan, N.; Nath, G.; Pritchard, T. Critical comparative assessment of a novel approach for multi-mineral modeling in shale gas: results from an evaluation study of marcellus shale. *SPE Unconventional Resources Conference and Exhibition-Asia Pacific*. 2013.
(37) Hofmann, A.; Rigollet, C.; Portier, E.; Burns, S. Gas shale characterization - results of the mineralogical, lithological and geochemical analysis of Cuttings samples from radioactive silurian shales of a Palaeozoic Basin, SW Algeria. *North Africa Technical Conference and Exhibition. Soc. Petrol.* 2013, 1−6.
(38) Zhang, D. C.; Ranjith, P. G.; Perera, M. S. A. The brittleness indices used in rock mechanics and their application in shale hydraulic fracturing: a review. *J. Petrol. Sci.* **2016**, *143*, 158−170.
(39) Wei, Z. D. *Occurrence regularity of coal resources in Anhui Province and prediction of coal exploration.*; Geological Publishing House: Beijing (in Chinese with English abstract), 2012.
(40) Jiang, W. P.; Zhong, L. W.; Zhang, Q. Analysis of sedimentary environment of coal-bearing strata in Huainan mining area and its significance for coalbed methane development. *Proceedings of geological society of China and other academic conferences 7−8 (in Chinese with English abstract)*. 2007.
(41) Yu, H.; Dahi Taleghani, A.; Lian, Z. A new look at rock mechanical behavior from the mesoscale grain. *J. Petrol. Sci.* **2021**, *200*, 108373.
(42) Li, M.; Guo, Y.; Wang, H.; Li, Z.; Hu, Y. Effects of mineral composition on the fracture propagation of tight sandstones in the Zizhou area, east Ordos Basin, China. *J. Nat. Gas. Sci.* **2020**, *78*, No. 103334.
(43) Yu, K.; Qu, Z. H.; Yu, K. L.; Shao, C. J.; Li, G. Brittle minerals and depositional control of mudstone in coal measures form in well 1001 in Huainan mining area. *Coal Geology & Exploration* **2017**, *45*, 14−21 (in Chinese with English abstract).
(44) Zhuang, J. Oolite texture characteristics and formation environment of siderite. *Coalfield Geology and Exploration* **1988**, *02*, 7−10.
(45) Chen, S. J.; Du, Z. W.; Zhang, Z.; Zhang, H. W.; Xia, Z. G.; Feng, F. Effects of chloride on the early mechanics properties and microstructure of gangue-cemented paste backfill. *Constr. Build. Mater.* **2020**, *235* (2), No. 117504.

https://doi.org/10.1021/acsomega.3c07731
ACS Omega 2024, 9, 1375−1388

(46) Chen, S. J.; Du, Z. W.; Zhang, Z.; Yin, D. W.; Feng, F.; Ma, J. B. Effects of red mud additions on gangue-cemented paste backfill properties. *Powder Technol.* **2020**, *367* (5), 833−840.
(47) Cheng, J. H.; Li, R. X.; Qin, X. L.; Li, D. L.; Zhao, B. S.; Li, J. J.; Wang, N. Impact of diagenetic facies on mechanics properties of sandstone rock in low-permeability reservoirs: a case study of the upper paleozoic gas reservoir in east ordos basin. *Acta. Petro. Sin.* **2016**, *37*, 1256−1264.
(48) Handin, J.; Heard, H. C.; Magouirk, J. N. Effects of the intermediate principal stress on the failure of limestone, dolomite, and glass at different temperatures and strain rates. *J. Geophys.* **1967**, *72*, 611−640.
(49) Katahara, W. Clay mineral elastic properties. *SEG Annual Meeting Expanded Abstracts* **1996**, *15*, 1691−1694.
(50) Vanorio, T.; Prasad, M.; Nur, A. Elastic properties of dry clay mineral aggregates, suspensions and sandstones. *Geophy. J.* **2003**, *155*, 319−326.
(51) Li, H. T.; Li, X. L.; Fu, J. H.; Zhu, N. Q.; Chen, D. Y.; Wang, Y.; Ding, S. Experimental study on compressive behavior and failure characteristics of imitation steel fiber concrete under uniaxial load imitation steel ffber concrete under uniaxial load. *Constr. Build. Mater.* **2023**, *399* (8), No. 132599.
(52) Li, H. T.; Li, X. L.; Fu, J. H.; Gao, Z. L.; Chen, P.; Zhang, Z. B. Research on acoustic emission multi-parameter characteristics in the failure process of imitation steel fiber reinforced concrete. *Phys. Fluids.* **2023**, *35* (10), No. 107109.
(53) Chen, S. J.; Zhao, Z. H.; Feng, F.; Zhang, M. Z. Stress evolution of deep surrounding rock under characteristics of bi-modulus and strength drop. *J. Cent. South. Univ.* **2022**, *29* (2), 680−692.
(54) Li, S.; Chen, J. B.; Cao, Y.; Nie, X. R.; Li, Y.; Liu, J. Study on the influence factors of shale reservoir brittleness based on grey correlation analysis. *China Mining Magazine* **2019**, *28*, 169−174 (in Chinese with English abstract).
(55) Ju-Long, D. Control problems of grey systems. *Syst. Control. Lett.* **1982**, *1*, 288−294.
(56) Hao, X. J.; Chen, Z. Y.; Wei, Y. N.; Sun, Z. W.; Zhang, Q.; Jin, D. X.; Zhang, G. C. Dynamic Brittle Instability Characteristics of 2000m Deep Sandstone Influenced by Mineral Composition. *Shock. Vib.* **2021**, *2021*, 1−12.
(57) Li, Y.; Huang, W. H.; Jiu, B.; Sun, Q. L.; Che, Q. S. Modes of Occurrence and Origin of Minerals in Permian Coals from the Huainan Coalfield, Anhui, China. *Minerals-Basel* **2020**, *10*, 399.

https://doi.org/10.1021/acsomega.3c07731
ACS Omega 2024, 9, 1375−1388